

# An implicit scheme for steady two-dimensional free-surface flow calculation

## Un schéma implicite pour le calcul des écoulements permanents bidimensionnels à surface libre.

ATHANASIOS J. KLONIDIS, *Research Assistant, Department of Civil Engineering, Fluid Mechanics / Hydraulics Division, Democriton University of Thrace, Xanthi 671 00, Greece*

JOHANNES V. SOULIS, *Associate Professor, Department of Civil Engineering, Fluid Mechanics / Hydraulics Division, Democriton University of Thrace, Xanthi 671 00, Greece*

### ABSTRACT

An implicit numerical scheme has been developed and subsequently applied to calculate steady, two-dimensional depth averaged, free-surface flow problems. The implicit form of the scheme gives fast convergence. The scheme is second order accurate and unconditionally stable. The free-surface flow equations are transformed into a non-orthogonal, boundary-fitted coordinate system so as to simulate with accuracy irregular geometries. The model is used to analyze a wide variety of hydraulic engineering problems including subcritical flow in a converging-diverging flume, supercritical flow at a channel expansion with various Froude numbers, and mixed sub- and supercritical flow in a converging channel. The computed results are compared with measurements as well as with other numerical solutions and satisfactory agreement is achieved.

### RÉSUMÉ

Un schéma numérique implicite a été développé, puis appliqué au calcul des problèmes d'écoulements à surface libre à deux dimensions, moyennés sur la hauteur. La forme implicite du schéma permet une convergence rapide. Le schéma est précis au second ordre et inconditionnellement stable. Les équations de l'écoulement à surface libre sont transformées dans un système de coordonnées non orthogonales adaptées aux frontières pour représenter avec précision les géométries irrégulières. Le modèle est utilisé pour analyser une grande variété de problèmes d'ingénierie hydraulique y compris l'écoulement sous-critique dans un canal convergent-divergent, l'écoulement supercritique dans un élargissement de canal avec différents nombres de Froude, et l'écoulement mixte sous- et supercritique dans un canal convergent. Les résultats calculés sont comparés avec des mesures et avec d'autres solutions numériques, donnant un accord satisfaisant.

### Introduction

Most of hydraulic engineering problems can not be adequately treated using analytical solutions. In fact, most of two- and three-dimensional flow problems are described by system of non-linear partial differential equations for which analytical solutions are not available unless a great number of assumptions is made to simplify the problem and make the equations applicable only to idealized cases. The development of digital computers made it possible for many numerical methods to be applied in complicated flow problems. With the rapid improvement of computer technology, during the last 15 years, the numerical solution of fluid dynamics problems has become a fundamental prerequisite.

From a plethora of numerical techniques those that are applied to one-dimensional (1D) open-channel flow problems are very common and have been in use for many years. However, most flows in nature are three-dimensional (3D). The description of such flows using two-dimensional (2D) depth-averaged mathematical models, is possible under certain conditions. The assumption of invariable flow properties along the vertical direction leads to some loss of information concerning the vertical velocity distribution. This lost information may be insignificant where turbulent mixing due to bed roughness allows an approximately uniform vertical velocity distribution. On the other hand, the assumption of hydrostatic pressure distribution seems to be valid for smooth water surfaces. Finite-difference, finite-element and finite-volume numerical schemes are available for two-dimensional, steady, viscous, free-surface flow calculations. Among them, the explicit

ones are more popular because of the convenience they provide in comprehension and programming. However, most of these techniques are slow in their convergence because of the limitation imposed to the time step in order to ensure the stability of the scheme. From the computational time point of view, implicit techniques are the most efficient. The basic feature of these techniques is that the calculation of a variable at the unknown time level uses unknown values of the same variable at the same time level. Thus a system of equations is required to be solved. The great advantage of these techniques is that they are unconditionally stable, allowing the use of relatively large time steps, which are not strictly associated with the density of the computational grid. Furthermore, the introduction of a non-orthogonal, boundary-fitted coordinate system for the solution of 2D free surface flows in channels with compound geometry, Soulis (1991), eases the calculation of the required values on solid boundaries. Through a transformation, the quadrilaterals in the physical domain (global system) are mapped onto squares in the computational domain (local system). The governing flow equations are transformed so as their variables are referenced to the local coordinate system.

Kuipers and Vreugdenhill (1973) developed one of the first mathematical models capable of solving the 2D depth-averaged equations using a finite-difference scheme developed earlier by Leendertse (1967). Soulis (1991) developed an explicit finite-volume technique for either subcritical or supercritical flows. Predictions agreed well with measurements and/or other numerical method results. Earlier on, Soulis and Bellos (1989) presented

Revision received October 23, 2000. Open for discussion till February 28, 2002.

two finite-volume explicit numerical methods. The first method was obtained by using the well-known explicit numerical scheme of Mac Cormack, while the second one was obtained by solving the flow equations in integral form to series of finite-volumes with adjacent volumes sharing a common face. Both techniques gave good results but the convergence was relatively slow (sub-critical case). A depth-averaged flow model also developed by Molls and Chaudhry (1995). The model utilized an ADI Beam and Warming implicit scheme. A constant eddy-viscosity turbulence procedure was also incorporated into the model to approximate the turbulent Reynolds stresses. The model was applied successfully to various steady and unsteady flow problems. Finally, a 2D fast implicit bidiagonal scheme based on the Mac Cormack's predictor-corrector technique was developed by Panagiotopoulos and Soulis (1999). The main advantage of this model is that it requires the inversion of only the upper or lower block bidiagonal matrices. The model was used to analyze a wide variety of steady, subcritical and supercritical flow problems.

In the present study a general implicit numerical scheme has been developed and subsequently applied to steady, two-dimensional free-surface flow problems. The implicit form of the scheme gives fast convergence since it also allows the use of large time steps. The scheme is second order accurate, unconditionally stable. The free-surface flow equations are transformed into a non-orthogonal, boundary-fitted coordinate system so as to be possible for the model to handle various types of boundary conditions with accuracy. The credibility of the model is checked by applying it to various subcritical, supercritical and mixed sub- and super-critical free -surface flows. In all cases the computed results are compared with measurements as well as with other numerical solutions.

### Basic equations

Assuming that the flow is homogenous, incompressible, two-dimensional, viscous with hydrostatic pressure distribution and with absence of Coriolis and wind forced, the non-linear partial differential equations system used to describe the 2D, depth-averaged, free-surface flow is as follows:

$$\frac{\partial Q}{\partial t} + \frac{\partial F}{\partial x} + \frac{\partial G}{\partial y} = W \quad (1)$$

where the variables Q, F, G, and W are defined in matrix form as:

$$Q = \begin{Bmatrix} h \\ hv_x \\ hv_y \end{Bmatrix}, \quad F = \begin{Bmatrix} hv_x \\ hv_x^2 + gh^2/2 \\ hv_x v_y \end{Bmatrix},$$

$$G = \begin{Bmatrix} hv_y \\ hv_y v_x \\ hv_y^2 + gh^2/2 \end{Bmatrix}, \quad W = \begin{Bmatrix} 0 \\ gh(S_{ox} - S_{fx}) \\ gh(S_{oy} - S_{fy}) \end{Bmatrix}$$

In the above relations h represents the water depth,  $v_x$ ,  $v_y$  are the depth-averaged velocities along the longitudinal (x) and trans-

verse (y) direction respectively, g is the acceleration due to gravity and  $S_{ox}$ ,  $S_{oy}$  are the bottom slopes along the x and y direction respectively defined as:

$$S_{ox} = -\frac{\partial z}{\partial x}, \quad S_{oy} = -\frac{\partial z}{\partial y} \quad (2)$$

with z being the bottom elevation. The quantities  $S_{fx}$  and  $S_{fy}$  are the friction slopes in x and y directions, which are defined as:

$$S_{fx} = \frac{n^2 v_x \sqrt{v_x^2 + v_y^2}}{h^{4/3}}, \quad S_{fy} = \frac{n^2 v_y \sqrt{v_x^2 + v_y^2}}{h^{4/3}} \quad (3)$$

where n is the Manning's roughness coefficient. If instead of Manning's the Chezy's flow friction coefficient C is to be used, Eqs. (3) take the form:

$$S_{fx} = \frac{v_x \sqrt{v_x^2 + v_y^2}}{hC^2}, \quad S_{fy} = \frac{v_y \sqrt{v_x^2 + v_y^2}}{hC^2} \quad (4)$$

The above definition of friction slopes assumes that only the bottom shear stress is taken into account for the calculation of the energy losses. Side-wall friction is assumed to be negligible (free slip walls). The depth-integrated effective stress has also been neglected.

### Transformation of flow equations

According to the present finite-volume scheme, quadrilaterals resulting from the formation of the physical domain are mapped onto squares in the computational domain. This is accomplished through independent transformations from the Cartesian (x, y) to the local coordinate system ( $\xi$ ,  $\eta$ ). A primary element (quadrilateral) in the physical domain consists of four nodes located in the corners. In the local coordinate system the resultant secondary element is a square, which is comprised of four primary elements. This secondary element consists of eight nodes, four of which are located in the corners and the remaining in the middle of each side, see Fig. 1. The secondary element centre is the point where the local coordinate system is initiated ( $\xi = 0$ ,  $\eta = 0$ ) with  $\xi$  and  $\eta$  ranging between  $-1 \leq \xi \leq 1$  and  $-1 \leq \eta \leq 1$ . The resulting grid covers the whole flow field. The potential of this technique focuses on the ease and accuracy with which various boundary con-

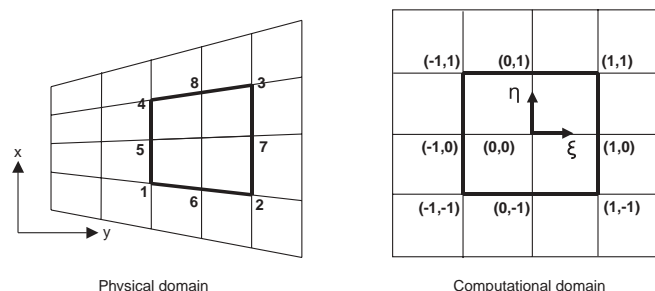


Fig. 1. Distorted squares mapped onto squares.

ditions are applied. Also, the proposed transformation is consistent with many finite difference schemes using central differences in space.

Let  $[J]$  be the transformation matrix from the physical to local coordinate system defined as, Soulis (1991):

$$[J] = \begin{Bmatrix} \frac{\partial x}{\partial \xi} & \frac{\partial x}{\partial \eta} \\ \frac{\partial y}{\partial \xi} & \frac{\partial y}{\partial \eta} \end{Bmatrix} \quad (5)$$

and the reverse matrix  $[J]^{-1}$  is:

$$[J]^{-1} = \begin{Bmatrix} \frac{\partial \xi}{\partial x} & \frac{\partial \xi}{\partial y} \\ \frac{\partial \eta}{\partial x} & \frac{\partial \eta}{\partial y} \end{Bmatrix} \quad (6)$$

The following relations hold

$$\begin{aligned} \frac{\partial x}{\partial \xi} &= J^{-1} \frac{\partial \eta}{\partial y}, & \frac{\partial x}{\partial \eta} &= -J^{-1} \frac{\partial \xi}{\partial y}, \\ \frac{\partial y}{\partial \xi} &= -J^{-1} \frac{\partial \eta}{\partial x}, & \frac{\partial y}{\partial \eta} &= J^{-1} \frac{\partial \xi}{\partial x} \end{aligned} \quad (7)$$

where  $J^{-1} = \frac{\partial x}{\partial \xi} \frac{\partial y}{\partial \eta} - \frac{\partial x}{\partial \eta} \frac{\partial y}{\partial \xi}$  is the determinant of matrix  $[J]$

The velocity components  $v_\xi, v_\eta$  in the computational domain are related to  $v_x, v_y$  in the physical domain with the following relation:

$$\begin{Bmatrix} v_\xi \\ v_\eta \end{Bmatrix} = [J]^{-1} \begin{Bmatrix} v_x \\ v_y \end{Bmatrix} \quad (8)$$

Under the aforementioned transformation into the local coordinate system, Eq. (1) takes the form:

$$\frac{\partial \hat{Q}}{\partial t} + \frac{\partial \hat{F}}{\partial \xi} + \frac{\partial \hat{G}}{\partial \eta} = \hat{W} \quad (9)$$

where the variables  $\hat{Q}, \hat{F}, \hat{G}, \hat{W}$  are in matrix form:

$$\hat{Q} = \begin{Bmatrix} J^{-1}h \\ J^{-1}hv_x \\ J^{-1}hv_y \end{Bmatrix}, \quad \hat{F} = \begin{Bmatrix} J^{-1}hv_\xi \\ J^{-1}(hv_\xi v_x + \frac{\partial \xi}{\partial x} \frac{gh^2}{2}) \\ J^{-1}(hv_\xi v_y + \frac{\partial \xi}{\partial y} \frac{gh^2}{2}) \end{Bmatrix}, \quad (10)$$

$$\hat{G} = \begin{Bmatrix} J^{-1}hv_\eta \\ J^{-1}(hv_\eta v_x + \frac{\partial \eta}{\partial x} \frac{gh^2}{2}) \\ J^{-1}(hv_\eta v_y + \frac{\partial \eta}{\partial y} \frac{gh^2}{2}) \end{Bmatrix}, \quad \hat{W} = \begin{Bmatrix} 0 \\ J^{-1}gh(S_{ox} - S_{fx}) \\ J^{-1}gh(S_{oy} - S_{fy}) \end{Bmatrix}$$

### Numerical scheme

Recalling the 2D free-surface flow equation transformed into the local coordinate system (Eq. 9) and solving for  $\partial \hat{Q} / \partial t$ , it becomes:

$$\frac{\partial \hat{Q}}{\partial t} = -\frac{\partial \hat{F}}{\partial \xi} - \frac{\partial \hat{G}}{\partial \eta} + \hat{W} \quad (11)$$

If the Taylor series expansion is used for  $\hat{Q}$  then

$$\hat{Q}^{n+1} = \hat{Q}^n + \frac{\partial \hat{Q}}{\partial t} \Delta t + 0.5 \Delta t^2 \frac{\partial^2 \hat{Q}}{\partial t^2} \quad \text{or} \quad \Delta \hat{Q}^{n+1} = \frac{\partial \hat{Q}}{\partial t} \Delta t \quad (12)$$

where  $\Delta \hat{Q}^{n+1} = \hat{Q}^{n+1} - \hat{Q}^n$

From Eqs. (12) and (11)

$$\Delta \hat{Q}^{n+1} = -\Delta t \left( \frac{\partial \hat{F}^{n+1}}{\partial \xi} + \frac{\partial \hat{G}^{n+1}}{\partial \eta} - \hat{W}^n \right) \quad (13)$$

The terms  $\hat{F}$  and  $\hat{G}$  can be linearized by expanding to Taylor series as:

$$\begin{aligned} \hat{F}^{n+1} &= \hat{F}^n + \frac{\partial \hat{F}}{\partial t} \Delta t + 0.5 \Delta t^2 \frac{\partial^2 \hat{F}}{\partial t^2} = \hat{F}^n + \frac{\partial \hat{F}}{\partial \hat{Q}} \frac{\partial \hat{Q}}{\partial t} \Delta t \quad \text{or} \\ \hat{F}^{n+1} &= \hat{F}^n + \hat{A}^n \Delta \hat{Q}^{n+1} \end{aligned} \quad (14)$$

similarly

$$\hat{G}^{n+1} = \hat{G}^n + \hat{B}^n \Delta \hat{Q}^{n+1} \quad (15)$$

where  $\hat{A} = \frac{\partial \hat{F}}{\partial \hat{Q}}$  and  $\hat{B} = \frac{\partial \hat{G}}{\partial \hat{Q}}$  are the Jacobian matrices defined as,

Molls and Chaudhry (1995):

$$\hat{A} = \begin{Bmatrix} 0 & \xi_x & \xi_y \\ gh\xi_x - v_x v_\xi & v_\xi + v_x \xi_x & v_x \xi_y \\ gh\xi_y - v_y v_\xi & v_y \xi_x & v_y \xi_y \end{Bmatrix},$$

$$\hat{B} = \begin{Bmatrix} 0 & \eta_x & \eta_y \\ gh\eta_x - v_x v_\eta & v_\eta + v_x \eta_x & v_x \eta_y \\ gh\eta_y - v_y v_\eta & v_y \eta_x & v_y \eta_y \end{Bmatrix}$$

The spatial derivatives of Eqs. (14) and (15) along  $\xi$  and  $\eta$ , respectively, give:

$$\frac{\partial \hat{F}^{n+1}}{\partial \xi} = \frac{\partial \hat{F}^n}{\partial \xi} + \frac{\partial(\hat{A}^n \Delta Q^{n+1})}{\partial \xi} \quad (16)$$

$$\frac{\partial \hat{G}^{n+1}}{\partial \eta} = \frac{\partial \hat{G}^n}{\partial \eta} + \frac{\partial(\hat{B}^n \Delta Q^{n+1})}{\partial \eta} \quad (17)$$

Combining Eqs. (16) and (17) with Eq. (13) and substituting the spatial derivatives with central differences, the following equation is derived:

$$\begin{aligned} \Delta \hat{Q}^{n+1} = & -\frac{\Delta t}{2\Delta \xi} (\hat{F}_{i,j+1}^n - \hat{F}_{i,j-1}^n) \\ & - \frac{\Delta t}{2\Delta \xi} (\hat{A}_{i,j+1}^{n*} - \hat{A}_{i,j-1}^{n*}) \Delta \hat{Q}^{n+1} \\ & - \frac{\Delta t}{2\Delta \eta} (\hat{G}_{i+1,j}^n - \hat{G}_{i-1,j}^n) - \frac{\Delta t}{2\Delta \eta} (\hat{B}_{i+1,j}^{n*} \\ & - \hat{B}_{i-1,j}^{n*}) \Delta \hat{Q}^{n+1} + \hat{W}_{i,j}^n \end{aligned} \quad (18)$$

The dots in the above equation indicate that the terms (i.e.  $\hat{A}_{i,j+1}^n$ ) operate also on the factors to the right.

If  $\delta$  denotes central difference, then the above equation becomes:

$$\begin{aligned} \Delta \hat{Q}^{n+1} + \frac{\Delta t}{2} \frac{\delta \hat{A}^n}{\Delta \xi} \Delta \hat{Q}^{n+1} + \frac{\Delta t}{2} \frac{\delta \hat{B}^n}{\Delta \eta} \Delta \hat{Q}^{n+1} = \\ -\frac{\Delta t}{2} \left( \frac{\delta \hat{F}^n}{\Delta \xi} + \frac{\delta \hat{G}^n}{\Delta \eta} - \hat{W} \right) \text{ or} \\ \left( I + \frac{\Delta t}{2} \frac{\delta \hat{A}^n}{\Delta \xi} + \frac{\Delta t}{2} \frac{\delta \hat{B}^n}{\Delta \eta} \right) \Delta \hat{Q}^{n+1} = -\frac{\Delta t}{2} \left( \frac{\delta \hat{F}^n}{\Delta \xi} + \frac{\delta \hat{G}^n}{\Delta \eta} - \hat{W} \right) \end{aligned} \quad (19)$$

where  $I$  is the identity matrix.

Approximate factorisation of Eq. (19) yields:

$$\begin{aligned} \left( I + \frac{\Delta t}{2} \frac{\delta \hat{A}^n}{\Delta \xi} \right) \left( I + \frac{\Delta t}{2} \frac{\delta \hat{B}^n}{\Delta \eta} \right) \Delta \hat{Q}^{n+1} = \\ -\frac{\Delta t}{2} \left( \frac{\delta \hat{F}^n}{\Delta \xi} + \frac{\delta \hat{G}^n}{\Delta \eta} - \hat{W} \right) \end{aligned} \quad (20)$$

Eq. (20) is implemented by the following sequence:

$$\left( I + \frac{\Delta t}{2} \frac{\delta \hat{A}^n}{\Delta \xi} \right) \Delta \hat{Q}^* = -\frac{\Delta t}{2} \left( \frac{\delta \hat{F}^n}{\Delta \xi} + \frac{\delta \hat{G}^n}{\Delta \eta} - \hat{W} \right) \quad 1^{st} \text{ step} \quad (21)$$

$$\left( I + \frac{\Delta t}{2} \frac{\delta \hat{B}^n}{\Delta \eta} \right) \Delta \hat{Q}^{n+1} = \Delta \hat{Q}^* \quad 2^{nd} \text{ step} \quad (22)$$

$$\hat{Q}^{n+1} = \hat{Q}^n + \Delta \hat{Q}^{n+1} \quad 3^{rd} \text{ step} \quad (23)$$

Eqs. (21)-(23) constitute the implicit numerical formulation of Eq. (9). The values of the unknown variables at every point of the field are obtained by solving a block tridiagonal system. The scheme is 2-order accurate and unconditionally stable. The computations proceed as follows:

1. Firstly, step1 sweeps the computational domain along the  $\xi$ -direction. The solution of the block tridiagonal system determines the value of  $\Delta \hat{Q}^*$  at every grid point of the flow field except for the points lying on the solid boundaries, as well as on the inlet grid line and on the outlet grid line. The types of boundary conditions used by the model are discussed in subsequent section.
2. Boundary conditions are applied to determine the value of  $\Delta \hat{Q}^*$  on the upper and lower solid boundary.
3. In step 2 the scheme sweeps the flow field along the  $\eta$ -direction. The solution of the resulting block tridiagonal system determines the value of  $\Delta \hat{Q}^{n+1}$  at every grid point of the flow field except for those grid points lying on the inlet and outlet.
4. Finally, step 3 takes over to calculate the values of  $\hat{Q}^{n+1}$  at every computed grid point.
5. Inlet and outlet boundary conditions are then applied.
6. The iterations continue until the convergence criterion related to the average percentage velocity is satisfied. If

$$v = \sqrt{v_x^2 + v_y^2}$$

is the resultant velocity, the iterations stop when  $(v^{n+1} - v^n)/v^n \times 100 < \text{ERROR}$ , where ERROR is a predefined value usually not less than  $10^{-6}$ .

### Boundary conditions

The law of the wall is used for the application of solid boundaries. According to this law the value of the velocity component normal to the solid boundary is set equal to zero. In addition the values of  $\Delta \hat{Q}^*$  along the upper and lower solid boundary are determined by extrapolation from the interior grid nodes.

For supercritical case the velocities  $v_x$ ,  $v_y$  and the water depth  $h$  are specified at the inlet while at the outlet these variables are free to change and their values are extrapolated from the interior grid nodes. For subcritical case the terms  $h v_x$  and  $h v_y$  are specified at the inlet, while the water depth  $h$  is extrapolated from the interior

nodes. The flow velocities  $v_x$ ,  $v_y$  are calculated as:  $v_x = hv_x / h$  and  $v_y = hv_y / h$ . At the outlet the water depth  $h$  is fixed while the  $v_x$  and  $v_y$  velocities are extrapolated from the interior grid points. Finally, if the flow is subcritical at the inlet and supercritical at the outlet (mixed flow) the water depth  $h$  is fixed at the inlet as well as at the outlet while the  $v_x$  and  $v_y$  velocities are extrapolated from the interior grid points. This condition for the mixed flow type was proved to be valid for the currently reported test case. In general for mixed flow type conditions (subcritical entrance) the water depth at the outlet must be specified, while at the inlet one must specify the total available head as well as the flow angle.

### Courant-Friedrichs-Lewy condition

Since the implicit scheme described above is a time-marching method, the time step  $\Delta t$  must be specified to advance the solution. The use of Courant-Friedrichs-Lewy (CFL) criterion is an effective way of choosing an appropriate time step. For every point  $i, j$  of the computational domain  $\Delta t$  is determined so as

$$\Delta t = \min(\Delta t_1, \Delta t_2) \quad \text{where} \quad \Delta t_1 = \text{CN} \left( \frac{1}{2} \frac{\Delta x}{|v_x| + c} \right)$$

$$\text{and} \quad \Delta t_2 = \text{CN} \left( \frac{1}{2} \frac{\Delta y}{|v_y| + c} \right) \quad (24)$$

In the above relations  $c = \sqrt{gh}$  is the wave speed and CN is the Courant number.

### Artificial viscosity

High order implicit schemes, like the present one, often produce numerical instabilities indicated by oscillations near discontinuous solid boundaries (i.e. large expansions-contractions, bends etc). These instabilities which are due to dispersion errors, can be effectively damped by introducing a second order artificial viscosity. Thus the following artificial viscosity, Hoffman and Chiang (1993), is added to the  $Q$  values derived from Eq. (23) following the inverse transformation procedure:

$$AV = DC [(Q_{i,j+1} - 2Q_{i,j} + Q_{i,j-1}) + (Q_{i+1,j} - 2Q_{i,j} + Q_{i-1,j})] \quad (25)$$

where DC is a dissipation constant. The solution will be stable only if  $0 < DC \leq 0.125$ .

### Model applications

In order to test its validity, the current model was applied to steady subcritical, supercritical and mixed sub- and supercritical flow problems. In all cases the computed results were compared with available measurements and other numerical methods results.

#### Converging-Diverging Subcritical Flow after Soulis (1997)

In this section the versatility of the model in subcritical flows is verified by comparing it with available measurements, Soulis (1997) as well as with results of another implicit numerical scheme, Panagiotopoulos and Soulis (1999). Such flow was developed in a linearly converging-diverging laboratory flume. Fig. 2 shows the schematic plan view and geometry of the tested flume. At the inlet flow region the width  $b$  is equal to 0.25 m. Thereafter the flume converges (at an axial distance of 0.5 m) and at the axial distance of 1.15 m the width takes half the value at entrance i.e. 0.125 m with a contraction angle of  $10.88^\circ$ . The throat area extends to a distance of 0.30 m where the width keeps a constant value of 0.125 m. At an axial distance of 0.95 m away from the point of initial convergence, the flume side wall diverges with an expansion angle of  $21.037^\circ$ . Eventually, 1.275 m away from the point of initial convergence, the width takes again the value of 0.25 m. The value of Chezy's flow friction coefficient was estimated to be 120.0, which agrees with published values for glass sided-iron bed flume. An  $8 \times 47$  computational grid was used for the simulation of flume's geometry, while boundary conditions with respect to subcritical flows were imposed. The optimum artificial viscosity value was estimated after numerical experimentation to be 0.11 and the Courant number was set equal to 0.4

A discharge  $Q$  of 20.58 lit/sec was applied, while the downstream flow depth  $h_2$  was 0.286 m and the bed slopes  $S_{0x}$ ,  $S_{0y}$  were equal to  $0 \text{ ‰}$ . Velocities and water depths were measured at various positions throughout the flow field, Soulis (1997). There were 6 (six) hypothetical streamlines, see Fig. 2. In Figs. 3 to 6 the computed results of flow depths and axial velocities along the stream-

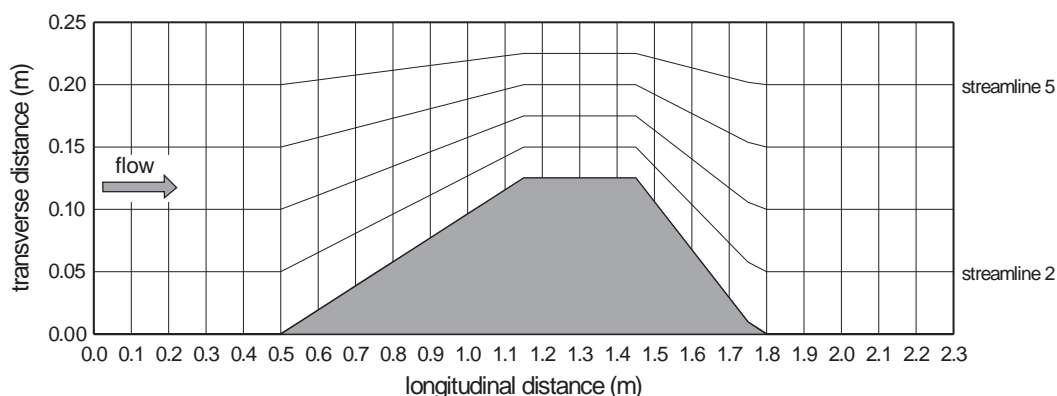


Fig. 2. Converging-diverging flow geometry with "streamlines". Subcritical flow.

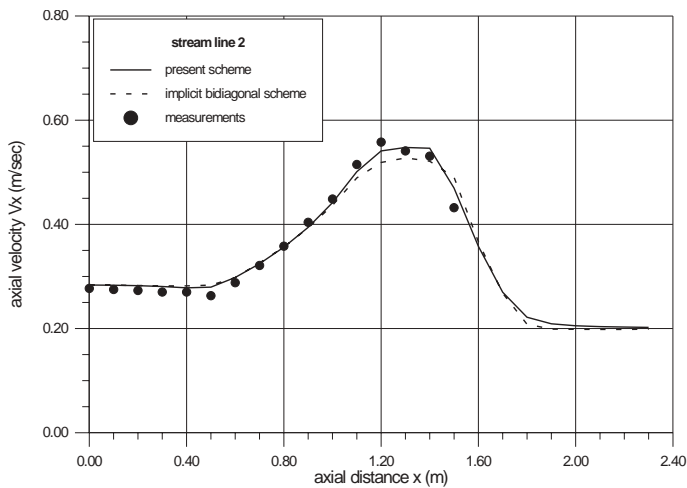


Fig. 3. Axial flow velocity comparison between current method predictions, implicit bidiagonal scheme predictions, Panagiotopoulos and Soulis (1999), and measurements for the converging-diverging flume along streamline 2.

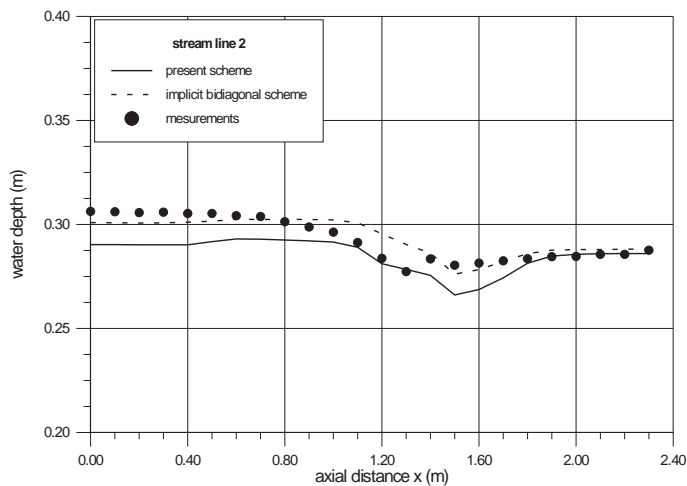


Fig. 4. Water depth comparison between current method predictions, implicit bidiagonal scheme predictions, Panagiotopoulos and Soulis (1999) and measurements for the converging-diverging flume along streamline 2.

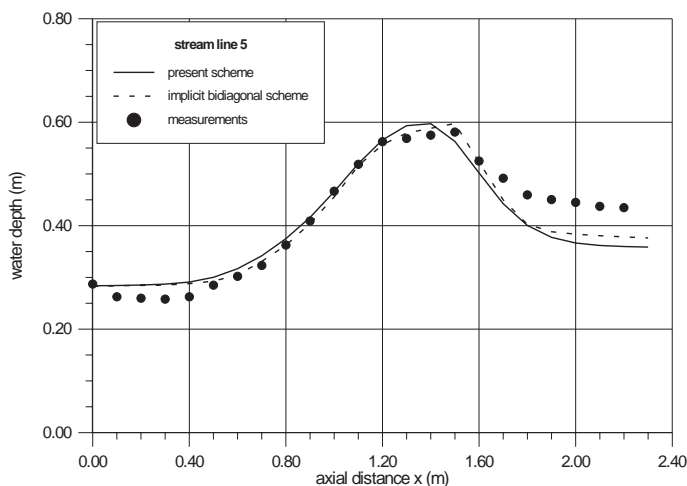


Fig. 5. Axial flow velocity comparison between current method predictions, implicit bidiagonal scheme predictions, Panagiotopoulos and Soulis (1999) and measurements for the converging-diverging flume along streamline 5.

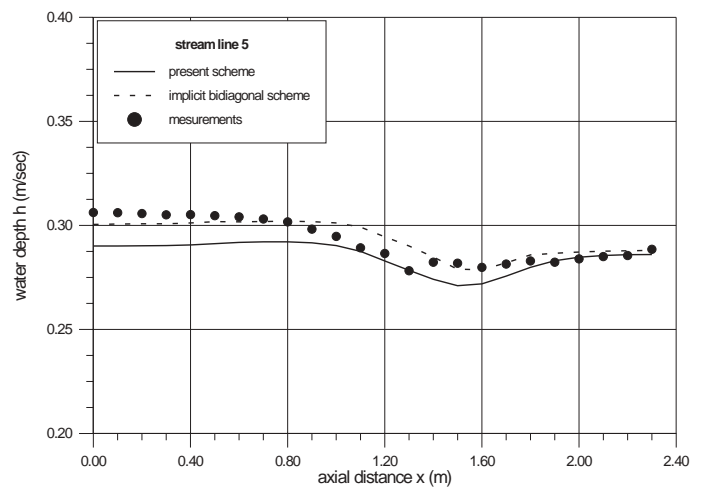


Fig. 6. Water depth comparison between current method predictions, implicit bidiagonal scheme predictions, Panagiotopoulos and Soulis (1999) and measurements for the converging-diverging flume along streamline 5.

lines 2 and 5, respectively are compared with the measured ones as well as with the results of an implicit scheme, Panagiotopoulos and Soulis (1999). The comparison seems to be satisfactory particularly in the converging part of the flume as well as in the narrow flow region. Also, both numerical schemes results agree to each other more as far as the velocity comparison is concerned than in water depths. Unfortunately, the velocities near the diverging part (streamline 2) were not possible to be measured. This was due to the presence of high viscous flow in that region where flow reversal was recorded. Velocities were measured near the upper straight wall (streamline 5). Also, a discrepancy appears between measured and computed velocities in the diverging part of the flume, see Fig. 5, indicating the weakness of the tested model to respond with success to 3D turbulent flows.

#### Channel expansion at $Fr = 2.0$ after Rouse et al (1951)

Rouse et al (1951) performed measurements in a channel expansion where the flow was supercritical. The current model computed results are compared with the measurements as well as with the results of an explicit numerical scheme, Soulis (1991). The channel expansion, shown in Fig. 7, was designed for an entrance Froude number of 2.0. The channel geometry is given by the formula:

$$\frac{y}{b_1} = \frac{1}{2} \left( \frac{x}{2b_1} \right)^{3/2} + \frac{1}{2}$$

where  $b_1$  is the inlet width equal to 10.0 m. The channel is symmetrical about the center line but for computational purposes only the upper half portion was modeled. The bottom slopes  $S_{0x}$  and  $S_{0y}$  were set equal to  $0.0 \text{ } ^\circ/_{00}$ . The inlet flow depth  $h_1$  was set equal to 1.0 m, while the flow discharge  $Q$  was  $31.316 \text{ m}^3/\text{sec}$ . The above conditions were consistent with the requirement of  $Fr = 2.0$  at the inlet. No flow boundaries were applied at the outlet (supercritical flow). The Manning's roughness coefficient  $n$  was

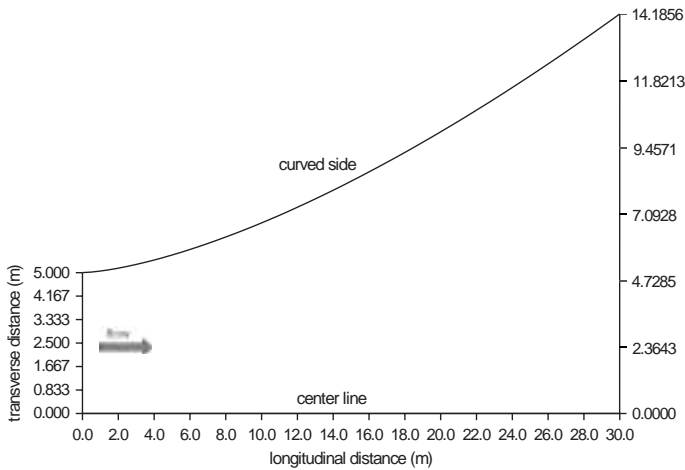


Fig. 7. Channel geometry for  $Fr = 2.0$  after Rouse et al (1951).

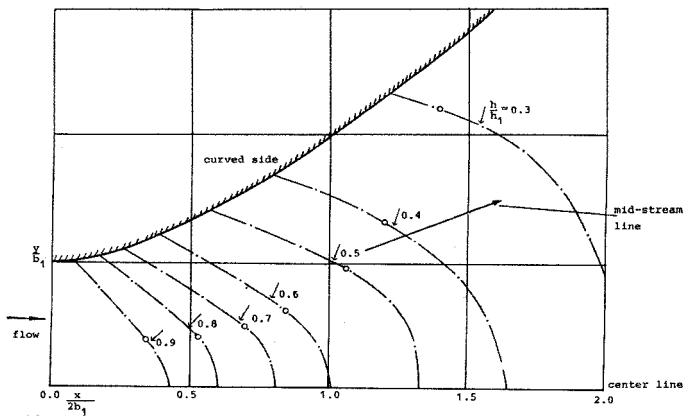


Fig. 8. Measured iso-depth (m) contours for the Rouse et al channel (1951) at  $Fr = 2.0$ .

given the value of 0.012. The flow was modeled using  $7 \times 61$  grid points. A value of 1.5 was used for the Courant number while the optimum value of artificial viscosity was estimated to be 0.12. Fig. 8 shows the flow iso-depth (m) contours as these were measured by Rouse et al. Fig. 9 shows a contour plot of computed by the current model flow iso-depths. Comparison between two method predictions and measurements along the centerline, mid-streamline and curved line is shown in Fig. 10. The comparisons are considered to be satisfactory. It must be noted that the predicted results are closer to each other than with the experimental data.

#### Channel expansion at $Fr = 4.0$ after Rouse et al (1951)

Measured data are also available for higher entrance Froude number,  $Fr = 4.0$ . The channel expansion shown in Fig. 11 was modeled for this number. The actual geometry in now given by the formula:

$$\frac{y}{b_1} = \frac{1}{2} \left( \frac{x}{4b_1} \right)^{3/2} + \frac{1}{2}$$

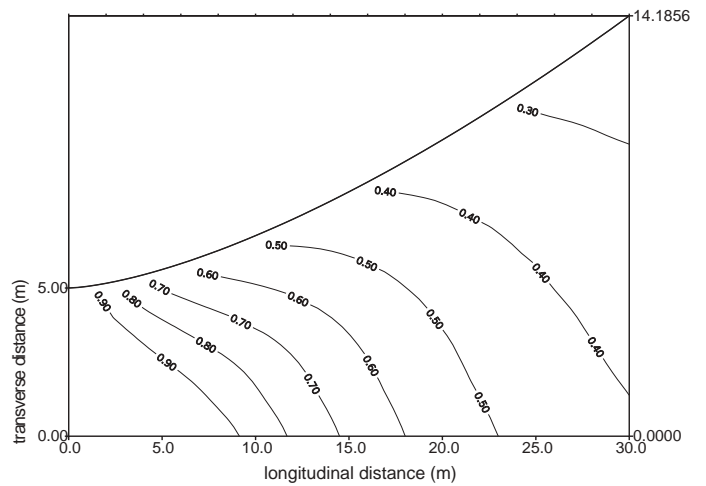


Fig. 9. Current method predicted iso-depth (m) contours for the Rouse et al channel (1951) at  $Fr = 2.0$ .

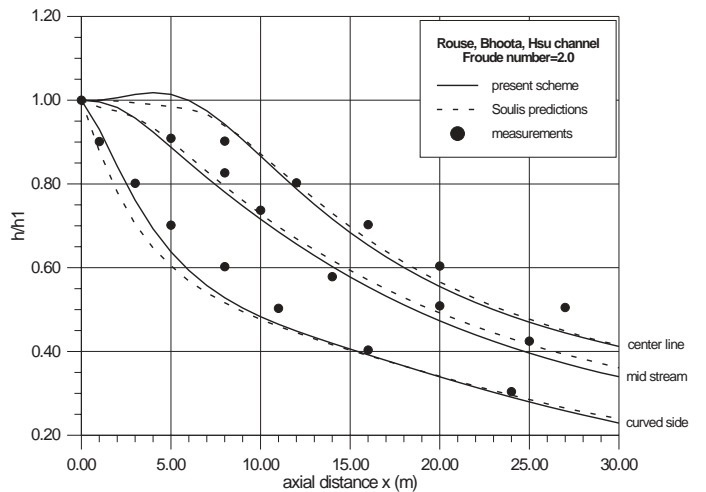


Fig. 10. Non-dimensionalized water depth comparison between current method predictions, Soulis predictions (1991) and measurements for the Rouse et al channel (1951) at  $Fr = 2.0$ .

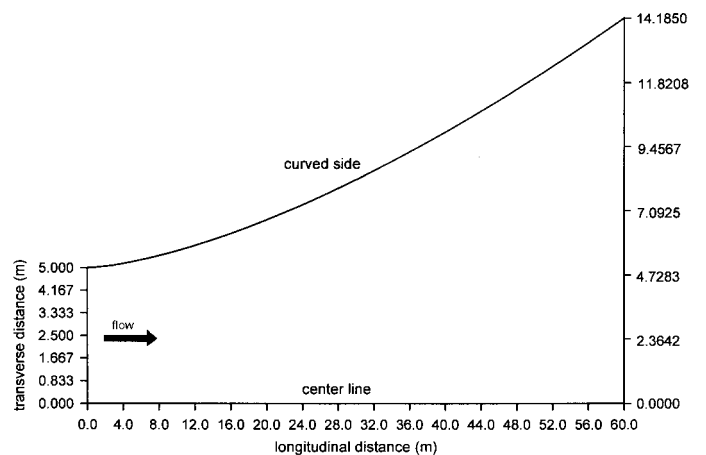


Fig. 11. Channel geometry for  $Fr = 4.0$  after Rouse et al (1951).

With the exception of inlet flow discharge which is now  $Q = 62.632 \text{ m}^3/\text{sec}$ , the other flow and geometry conditions remain the same as for  $Fr = 2.0$  test case. Fig. 12 shows the flow depth con-

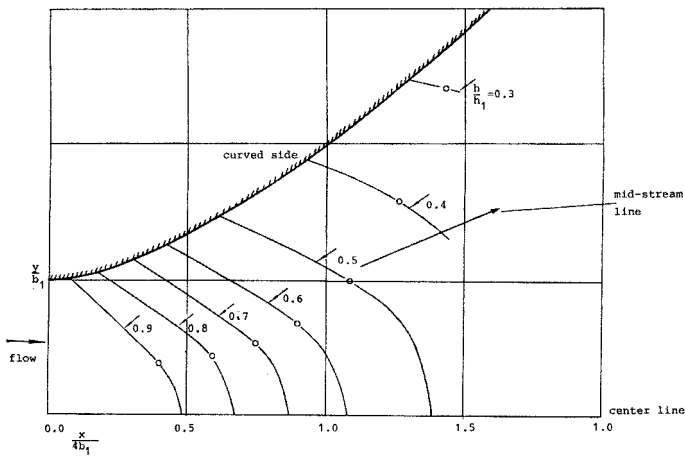


Fig. 12. Measured iso-depth (m) contours for the Rouse et al channel (1951) at  $Fr = 4.0$ .

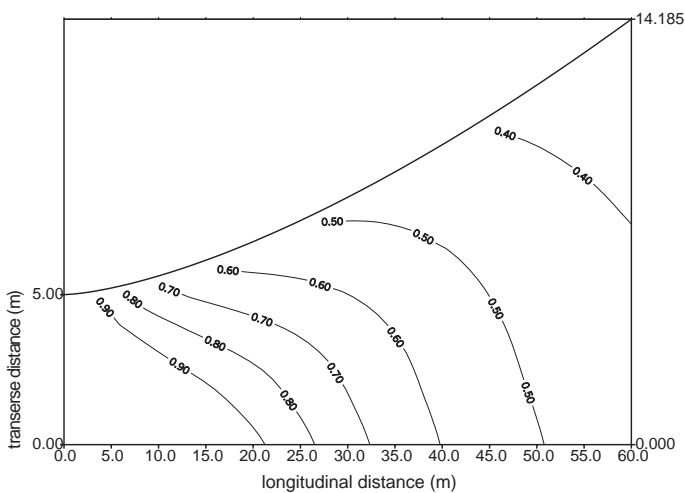


Fig. 13. Current method predicted iso-depth (m) contours for the Rouse et al channel (1951) at  $Fr = 4.0$ .

tours as these were measured by Rouse et al, while Fig. 13 shows a contour plot of computed flow iso-depths (m). Comparison between the two method predictions and measurements along the centerline, mid-streamline and curved line is shown in Fig. 14. Again the predicted results agree well with each other, while their agreement with the measurements seems to be satisfactory, particularly along the mid-streamline. The convergence history, shown in Fig. 15, indicates that after 120 iterations the current method's average percentage error reached the  $1.0 \times 10^{-5}$  region (compare with 222 iterations of Soulis explicit method).

#### Mixed flow in converging channel

Finally, the numerical model is tested in a mixed sub- and supercritical flow problem. This type of flow was created in a straight wall contraction by Coles and Shintaku (1943), at Lehigh University. They measured water-surface elevations, and presented their data in the form of water-surface contours. The mixed flow was subcritical at the inlet and throughout most of the contraction, while at the outlet slightly changed to supercritical. Molls and Chaudhry (1995) using an ADI scheme modeled this

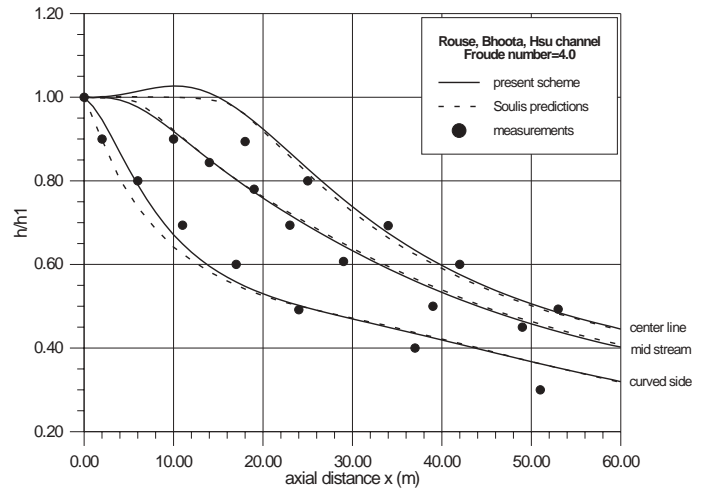


Fig. 14. Non-dimensionalized water depth comparison between current method predictions, Soulis predictions (1991) and measurements for the Rouse et al channel (1951) at  $Fr = 4.0$ .

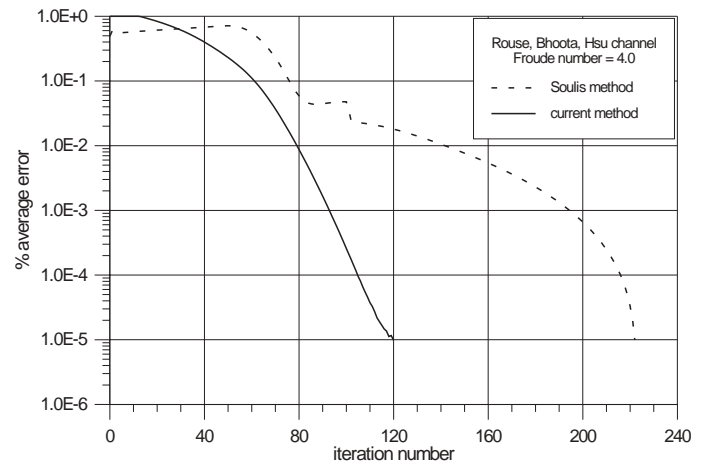


Fig. 15. Convergence history comparisons between current method predictions and Soulis (1991) method predictions for the Rouse et al channel (1951) at  $Fr = 4.0$ .

mixed flow problem. The current model computed results are compared with the available measurements as well as with the ADI numerical scheme results. The channel consisted of two straight rectangular sections joined by a 1.49 m long straight-walled contraction. The contraction side-walls angle was  $6^\circ$ . The inlet width was 0.629 m and the outlet one was 0.314 m., while the bottom slopes  $S_{0x}$  and  $S_{0y}$  were set equal to  $0.0/_{00}$ . The channel geometry is illustrated in Fig. 16. The flow conditions include flow discharge  $Q = 0.0451 \text{ m}^3/\text{sec}$ , constant upstream and downstream flow depths  $h_1 = 0.1762 \text{ m}$ ,  $h_2 = 0.1132 \text{ m}$ , respectively. Coles and Shintaku (1943) did not report Chezy's roughness coefficient for the channel contraction. However, Molls and Chaudhry (1995) after numerical experimentation found an optimum value of 84.1. For the proper simulation of the converging channel problem a  $21 \times 37$  grid was used. The Courant number was set equal to 1.5, while a value of 0.12 was used for the artificial viscosity. Fig. 17 shows the flow iso-depth (m) contours as they were measured by Coles and Shintaku (1943), while Fig. 18 shows the current method computed iso-depth (m) contours. At the downstream end of the contraction both predicted and measured contours bow toward the outlet boundary (0.126 iso-depth

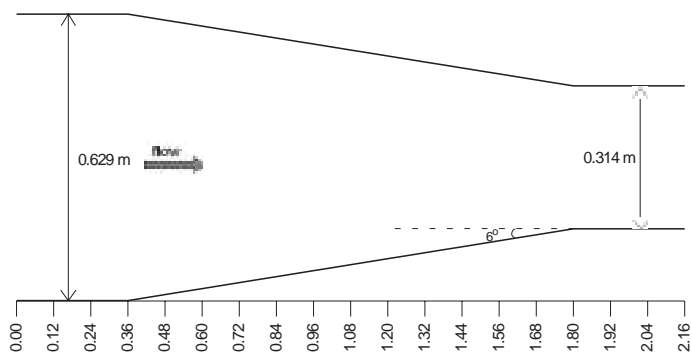


Fig. 16. Converging channel geometry for mixed flow type problem after Coles and Shintaku (1943).

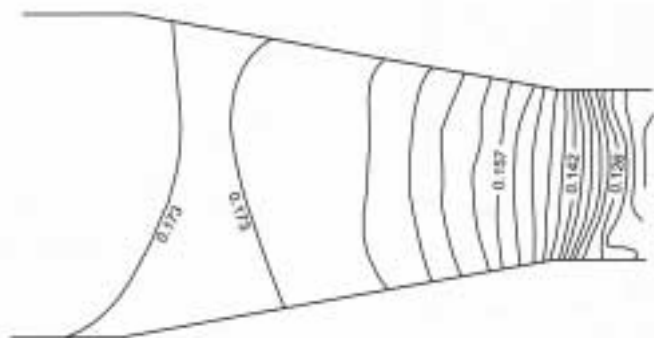


Fig. 17. Measured iso-depth (m) contours for the Coles and Shintaku channel (1943).

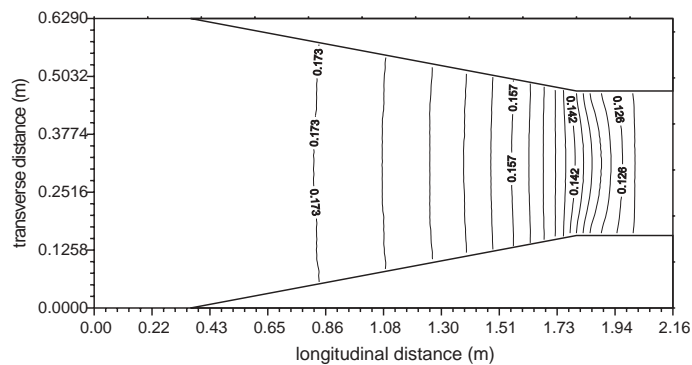


Fig. 18. Current method predicted iso-depth (m) contours for the Coles and Shintaku channel (1943).

contour), while at the upstream end the measured iso-depth (m) contour bows more toward the inlet boundary than the predicted one does (0.173 iso-depth contour). Also, in Fig. 19 the water depth computed both by the current model and the ADI scheme is compared with the measurements along the centerline. It is evident that the computed results agree very well with the experimental measurements. Varying the artificial viscosity slightly affected the solution. Finally, Fig. 20 shows the mixed flow type iso-Froude contours. Critical flow is attained few nodes upstream the outlet boundary.

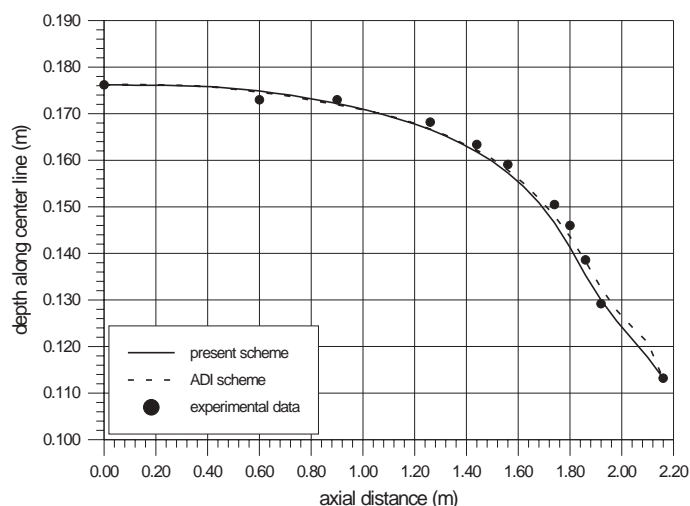


Fig. 19. Water depth comparison between current method predictions, ADI scheme predictions, Molls and Chaudhry (1995) and measurements for the converging channel, Coles and Shintaku (1943), along centerline.

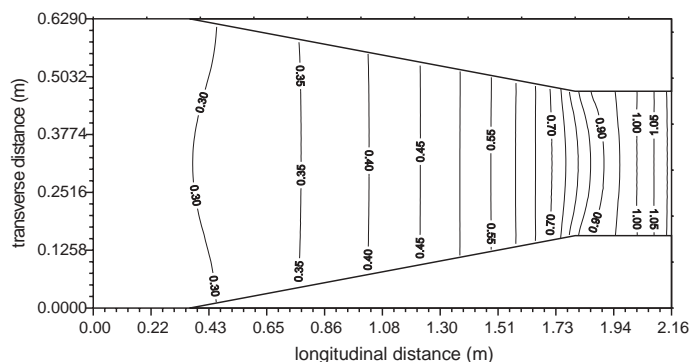


Fig. 20. Current method predicted iso-Froude contours for the Coles and Shintaku channel (1943).

## Conclusions

The partial differential equations describing the two-dimensional depth averaged free-surface flow are transformed into a body fitted non-orthogonal local coordinate system and solved using a second order implicit scheme resulted from the linearization of the governing equations. The numerical scheme is applied to steady state flow problems including subcritical, supercritical and mixed sub- and supercritical flows in converging-diverging channels and channels with expansions and/or contractions. The scheme is quite fast in convergence and flexible in simulating irregular geometry problems. Water surface depths and velocity comparisons with measurements and other numerical solutions show that the proposed method is comparatively accurate and reliable. However, in cases where the geometry combined with the flow conditions develop 3D, high-viscous flows (like in subcritical test case problem), it is difficult for the model to respond efficiently. Finally, the proposed scheme can be easily extended to simulate unsteady flows.

## Notations

AV	artificial viscosity
b	channel width
C	Chezy's flow friction coefficient
c	wave speed
CN	Courant number
DC	dissipation constant
ERROR	predefined small number
g	gravity acceleration
h	water depth
[J]	transformation matrix
$J^{-1}$	determinant of transformation matrix
n	Manning's flow friction coefficient
$S_{fx}, S_{fy}$	friction slopes along x- and y-direction
$S_{ox}, S_{oy}$	bottom slopes along x- and y-direction
t	time
$v_x, v_y$	depth-averaged velocity components in axial (x) and tangential (y) direction
$v_{\xi}, v_{\eta}$	local (computational) velocity components along $\xi$ - and $\eta$ - direction
v	resultant velocity
x, y	Cartesian coordinates
z	bottom elevation
A	(= $\partial F/\partial Q$ ) Jacobian matrix
B	(= $\partial G/\partial Q$ ) Jacobian matrix
$\delta$	central difference
$\Delta t$	time step
$\Delta x, \Delta y$	spatial steps in Cartesian coordinate system
$\Delta \xi, \Delta \eta$	spatial steps in local coordinate system
I	Identity matrix
$\xi, \eta$	local coordinates
1	upstream
2	downstream
n+1	unknown time level
*	intermediate value
^	transformed physical quantities

## References

- BERGER, R. C. and STOCKSTILL R. C. (1995). "Finite Element Model for High-Velocity Channels". Journal of Hydraulic Engineering, ASCE, pp 710-716.
- CHAKRAVARTHY, S. R. (1983). "Euler Equations-Implicit Schemes and Boundary Conditions". AIAA Journal, Vol. 21, No 5., pp 699-706.
- COLES, D. and SHINTAKU, T. (1943). "Experimental Relation Between Sudden Wall Angle Changes and Standing Waves in

- Supercritical Flow". B. S. Thesis, Lehigh University, Bethlehem, Pa.
- FENNEMA, R. J. and CHAUDHRY, M. H. (1989). "Implicit Methods for Two-Dimensional Unsteady Free-Surface Flows". Journal of Hydraulic Research, 27(3), pp 324-331.
- FOLKSTRA, C. (1977). "The Closure Problem for Depth-Averaged Two-Dimensional Flow". Proc., 17<sup>th</sup> Cong. of IAHR, Baden-Baden, Germany, Vol. 2, pp 247-256.
- HOFFMANN, K. A., CHIANG, S. T. (1993). "Computational Fluid Dynamics for Engineers". Engineering Education System, Wichita, Kansas, USA.
- MOLLS, T. and CHAUDHRY, M. H. (1995). "Depth-Averaged Open-Channel Flow Model". Journal of Hydraulic Engineering, ASCE, Vol 121, No 6, pp 453-465.
- MOLLS, T., CHAUDHRY, M. H. and KHAN, K. W. (1995). "Numerical Simulation of Two-Dimensional Flow Near a Spur-Dike". Advances in Water Resources, Vol. 18, No 4, pp 227-236.
- PANAGIOTOPOULOS, A. and SOULIS, J. V. (1999). "A Bidiagonal Scheme for Depth-Averaged, Free-Surface Flow Equations". Journal of Hydraulic Engineering, ASCE, Vol. and No to be appeared.
- ROUSE, H., BHOOTA, B. V. and HSU EN-YEN (1951). "Design of Channel Expansions". Trans. ASCE, 116, pp 347-363.
- SOULIS, J. V. and BELLOS, K. V. (1989). "Steady, Supercritical, Open-Channel Flow Computations". Proc. 6<sup>th</sup> Int. Conf. On Numerical Methods in Laminar and Turbulent Flow, Swansea.
- SOULIS, J. V. (1991). "A Numerical Method for Subcritical and Supercritical Open-Channel Flow Calculation". Int. J. for Numerical Methods in Fluids, Vol. 13, pp 437-464.
- SOULIS, J. V. (1997). "Prediction Performance of Quasi-2D and 2D Free-Surface Flow Algorithms". 7<sup>th</sup> Pan-hellenic Congress of the Greek Hydrotechnical Association, Patras.
- STUBBS, R. M. (1983). "Multiply-Gridding of the Euler Equations with an Implicit Scheme". AIAA Journal, C. P., pp 1883-1914.
- TINGSANCHALI, T. and MAHESWARAN, T (1990). "2-D Depth-Averaged Flow Computation Near Groyne". Journal of Hydraulic Engineering, ASCE, 116 (HY1), pp 71-86.
- WARMING, R. F. and BEAM, R. M. (1978). "An Implicit Factored Scheme for the Compressible Navier-Stokes Equations". AIAA Journal, Vol. 16, No 4, pp 393-402.
- WARMING, R. F. and BEAM, R. M. (1978). "On the Construction and Application of Implicit Factored Schemes for Conservation Laws". SIAMA. MS Proc., Vol. II.
- WEIYAN, T. (1992). "Shallow Water Hydrodynamics. Mathematical Theory and Numerical Solution for a Two-Dimensional System of Shallow Water Equations". Nanjing Research Institute of Hydrology and Water Resources, Nanjing, CHINA.